Effect of water-wall interaction potential on the properties of nanoconfined water

Pradeep Kumar[1], Francis W. Starr[2], Sergey V. Buldyrev[1,3], and H. Eugene Stanley[1]

[1]*Center for Polymer Studies and Department of Physics*

Boston University, 590 Commonwealth Avenue, Boston, MA 02215 USA

[2]*Department of Physics, Wesleyan University, Middletown, CT 06459 USA*

[3]*Department of Physics, Yeshiva University,*

500 West 185th Street, New York, NY 10033 USA

(Dated: last revised: February 6, 2008,   ksbs.tex)

Abstract

Much of the understanding of bulk liquids has progressed through study of the limiting case in which molecules interact via purely repulsive forces, such as a hard-core potential. In the same spirit, we report progress on the understanding of confined water by examining the behavior of water-like molecules interacting with planar walls via purely repulsive forces and compare our results with those obtained for Lennard-Jones (LJ) interactions between the molecules and the walls. Specifically, we perform molecular dynamics simulations of 512 water-like molecules which are confined between two smooth planar walls that are separated by 1.1 nm. At this separation, there are either two or three molecular layers of water, depending on density. We study two different forms of repulsive confinements, when the interaction potential between water-wall is (i) $1/r^9$ and (ii) WCA-like repulsive potential. We find that the thermodynamic, dynamic and structural properties of the liquid in purely repulsive confinements qualitatively match those for a system with a pure LJ attraction to the wall. In previous studies that include attractions, freezing into monolayer or trilayer ice was seen for this wall separation. Using the same separation as these previous studies, we find that the crystal state is not stable with $1/r^9$ repulsive walls but is stable with WCA-like repulsive confinement. However, by carefully adjusting the separation of the plates with $1/r^9$ repulsive interactions so that the effective space available to the molecules is the same as that for LJ confinement, we find that the same crystal phases are stable. This result emphasizes the importance of comparing systems only using the same effective confinement, which may differ from the geometric separation of the confining surfaces.

I. INTRODUCTION

Confinement of water in nanopores affects many properties of water, such as freezing temperature, crystal structure [1, 2, 3, 4, 5, 6], the glass transition temperature, and the position of the hypothesized liquid-liquid (LL) critical point [7, 8, 9, 10, 11]. Indeed, water confined in nanoscale geometries has received much recent attention, in part because of its importance in biology, engineering, geophysics and atmospheric sciences. The effects of different kinds of confinement have been studied, both using experiments and simulations [2, 3, 6, 12, 13, 14, 15, 16, 17, 18, 19].

Bulk supercooled water – water cooled below the equilibrium freezing temperature – shows many anomalous properties [1, 20, 21, 22]. Experiments find that at low temperatures, various response functions, such as isothermal compressibility and specific heat, increase sharply. There has been comparatively less research on confined water. Using the ST2 potential to model water confined between smooth plates [23], a LL phase transition has been proposed. A liquid-to-amorphous transition is seen in simulations of water using the TIP4P potential [24] confined in carbon nanotubes [3]. Recent theoretical work [25] suggests that hydrophobic Lennard-Jones (LJ) confinement shifts the LL transition to lower temperature and lower pressure compared to bulk water, a feature also found in simulations of water confined between hydrophobic plates [16].

Confinement is known to enhance solidification of molecules that are more or less spherical [26, 27, 28]. However, careful experiments on thin films of water show that water performs extremely well as a lubricant, suggesting that confined water may be more fluid than bulk water [29]. Recent experiments show that water in hydrophilic confinement, when cooled to very low T, does not freeze [9] – a phenomenon also supported by simulation studies [30, 31]. In contrast, simulations [2, 3, 6, 15, 16, 17] show that hydrophobically confined water does freeze into different crystalline structures, which do not have counterparts in bulk water. Indeed monolayer, bilayer and trilayer ice have all been found in simulations [2, 3, 6, 15, 16, 17]. Thus hydrophobic confinement seems to facilitate the freezing of water. However the reason for this facilitation is not yet fully understood. The hydrogen-bond interaction between water molecules is an order of magnitude stronger than Van der Waals attraction with the hydrophobic walls. Thus one may hypothesize that freezing in hydrophobic confinement depends critically on the separation between confining walls that

may distort or facilitate a particular crystalline structure, rather than on the weak details of the water-wall interaction potential. To test this hypothesis we perform molecular dynamics (MD) simulations of water in two different forms of repusive confinement. Specifically, we study:

- The $1/r^9$ repulsive part of the LJ potential studied in Ref. [16].

- The same potential used in Ref. [16] but truncated and shifted such that there is no attractive part in the potential, analogous to the Weeks-Chandler-Anderson (WCA) potential [32]. This potential allows us to examine the role, if any, the attractive part of the water-wall LJ potential plays in determining the thermodynamics and structure of confined water.

We compare the case when the water-wall interactions are purely repulsive ("repulsive confinement") with the studied case of pure LJ confinement [16]. We also compare the freezing in repulsive confinements with the freezing found when the water-wall interactions are represented by an LJ interaction ("LJ hydrophobic confinement") [2, 16].

This paper is organized as follows: In Sec. II, we provide details of our simulations and analysis methods. Simulation results for the liquid state are provided in Sec. III. In Sec. IV we discuss the freezing properties of our system.

II.   SIMULATION AND ANALYSIS METHODS

We perform MD simulations of a system composed of water-like molecules confined between two smooth walls. The molecules interact via the TIP5P pair potential [33] which, like the ST2 [34] potential, treats each water molecule as a tetrahedral, rigid, and non-polarizable unit consisting of five point sites [35]. The TIP5P potential predicts many of the anomalies of bulk water [36]. For example, TIP5P reproduces the density anomaly at $T = 277$ K and $P = 1$ atm and its structural properties compare well with experiments [33, 36, 37, 38, 39]. TIP5P is known to crystallize at high pressures [36] within accessible computer simulation time scales, and shows a "nose-shaped" curve of temperature versus crystallization time [36], a feature found in experimental data on water solutions [40].

In our simulations, $N = 512$ water molecules are confined between two smooth planar walls, as shown schematically in Fig. 1. The walls are located at $z_w = \pm 0.55$ nm (wall-wall

separation of 1.1 nm), which results in $\approx 2-3$ layers of water molecules. Periodic boundary conditions are used in the x and y directions, parallel to the walls.

We study two different forms of purely repulsive water-wall interaction. The first uses only the r^{-9} repulsive core, which we call the $1/r^9$ repulsive potential,

$$U\left(z-z_W\right) = 4\epsilon_{\mathrm{OW}}\left[\left(\frac{\sigma_{\mathrm{OW}}}{|z-z_W|}\right)^9\right]. \tag{1}$$

Here $|z-z_W|$ is the distance from the oxygen atom of a water molecule to the wall, while $\epsilon_{\mathrm{OW}} = 0.25$ kJ/mol and $\sigma_{\mathrm{OW}} = 0.25$ nm are potential parameters (Fig. 2). Similar but different parameter values were used in previous confined water simulations using the TIP5P interaction potential [16]. Specifically, in Ref. [16], the water-wall interaction was modelled using a 9-3 LJ potential with $\epsilon_{\mathrm{OW}} = 1.25$ kJ/mol and $\sigma_{OW} = 0.25$ nm. We choose a different ϵ_{OW} in the case of repulsive confinement so that the repulsion between the water and wall decays to almost zero where the 9-3 LJ -potential has a minimum.

The second purely repulsive potential uses both attractive and repulsive terms of the 9-3 LJ potential, but truncates and shifts the potential at the position of the minimum to create a repulsive potential that exactly mimics the repulsion of ref. [16], in analogy to the WCA potential,

$$U(z-z_W) = \begin{cases} 4\epsilon_{\mathrm{OW}}[(\frac{\sigma_{\mathrm{OW}}}{z-z_W})^9 - (\frac{\sigma_{\mathrm{OW}}}{z-z_W})^3] + \frac{8\epsilon_{\mathrm{OW}}}{3^{3/2}} & \text{if } |z-z_W| < 3^{1/6}\sigma_{\mathrm{OW}} \\ 0 & \text{if } |z-z_W| > 3^{1/6}\sigma_{\mathrm{OW}}, \end{cases}$$

where $\epsilon_{\mathrm{OW}} = 1.25$ kJ/mol and $\sigma_{OW} = 0.25$ nm. For the $1/r^9$ repulsive potential, we perform simulations for 56 state points, corresponding to seven temperatures $T = 220$ K, 230 K, 240 K, 250 K, 260 K, 280 K, and 300 K, and eight "geometric densities" $\rho_g = 0.60$ g/cm^3, 0.655 g/cm^3, 0.709 g/cm^3, 0.764 g/cm^3, 0.818 g/cm^3, 0.873 g/cm^3, 0.927 g/cm^3, and 0.981 g/cm^3 – the same as studied in Ref. [16]. The geometric values of density do not take into account the fact that the repulsive interactions of molecules with the walls increases the overall amount of available space, since the ϵ_{OW} parameter of the $1/r^9$ repulsive potential is smaller than the ϵ_{OW} used for the LJ confined system 2. For systems confined by LJ interactions, there is a well-defined preferred distance from the wall, making it relatively straightforward to evaluate the "effective" density of molecules confined by the attractive wall. In our system with only repulsive interactions, there is no such preferred distance, as emphasized by Fig. 2.

We can approximate the effective density by examining the local density $\rho(z)$ (Fig. 3). We utilize the fact that $\rho(z)$ has an inflection, and estimate the effective L_z by the location where the second derivative of $\rho(z) = 0$, or when first derivative of $\rho(z)$ has a maximum. We must also add to this value of L_z the molecular diameter of water(0.278 nm) to calculate the real space available along z-direction. The resulting "effective densities" are $\rho = 0.715$ g/cm^3, 0.777 g/cm^3, 0.829 g/cm^3, 0.890 g/cm^3, 0.949 g/cm^3, 1.000 g/cm^3, 1.060 g/cm^3, and 1.115 g/cm^3. We will use these effective densities throughout the paper, since they will be most comparable to the effective densities with LJ confinement.

For the WCA potential, we perform simulations for 32 state points, corresponding to 8 different temperatures and 4 different "geometric densities", 0.60 g/cm^3, 0.655 g/cm^3,0.709 g/cm^3,0.764 g/cm^3 respectively. These geometric densities correspond to "effective densities" 0.80 g/cm^3, 0.88g/cm^3, 0.95g/cm^3, 1.02g/cm^3 respectively. Note that these effective densities were calculated using the method described in [16, 23].

We control the temperature using the Berendsen thermostat with a time constant of 5 ps [41] and use a simulation time step of 1 fs, just as in the bulk system [36]. Water-water interactions are truncated at a distance 0.9 nm as discussed in Ref. [33].

III. THERMODYNAMICS AND STRUCTURE

One of the defining characteristics of water is the existence of a temperature of maximum density (TMD). Relative to bulk water – LJ confinement shifts the locus of the TMD to lower T by ≈ 40 K [16]. Additionally, the sharpness of the density maximum is markedly decreased in comparison to the bulk. Fig. 4 shows isochores of P for LJ confinement, $1/r^9$ repulsive confinement and WCA confinement, for similar densities. A TMD in this plot is coincident with the minimum in the isochore. For $1/r^9$ repulsive confinement, the minimum is very weak, but the location of the flatness in the isochore is near to that of the system with LJ confinement. This result suggests the the $1/r^9$ repulsive confinement further suppresses the structural ordering of the molecules that is known to be responsible to the presence of a density maximum. The TMD for the case of WCA confinement again appears at the same T as the $1/r^9$ repulsive confinement and LJ confinement cases but the isochore in the TMD region is flatter than for case the of LJ confinement confinemen. Hence both kinds of the repulsive confinement supprsess the structural ordering in lateral directions compared to the

case of bulk and LJ confinement. We further notice that the value of the lateral pressure $P_{\parallel}$ in the case of the LJ confinement approaches the value of $P_{\parallel}$ in case of WCA confinement at high temperatures. This behavior of $P_{\parallel}$ for LJ confinement should be expected since at very high temperatures the molecules will not feel the potential minimum of the water-wall interaction.

In order to compare the structural properties of repulsive confinement with those of LJ confinement, we calculate the lateral oxygen-oxygen radial distribution function (RDF) defined by

$$g_{\parallel}(r) \equiv \frac{1}{\rho^2 V} \sum_{i \neq j} \delta(r - r_{ij}) \left[\theta \left(|z_i - z_j| + \frac{\delta z}{2} \right) - \theta \left(|z_i - z_j| - \frac{\delta z}{2} \right) \right]. \qquad (2)$$

Here V is the volume, r_{ij} is the distance parallel to the walls between molecules i and j, z_i is the z-coordinate of the oxygen atom of molecule i, and $\delta(x)$ is the Dirac delta function. The Heaviside functions, $\theta(x)$, restrict the sum to a pair of oxygen atoms of molecules located in the same slab of thickness $\delta z = 0.1$ nm. The physical interpretation of $g_{\parallel}(r)$ is that $g_{\parallel}(r)2\pi r dr \delta z$ is proportional to the probability of finding an oxygen atom in a slab of thickness δz at a distance r (parallel to the walls) from a randomly chosen oxygen atom. In a bulk liquid, this would be identical to $g(r)$, the standard RDF.

Figure 5 shows the temperature and density dependence of the lateral oxygen-oxygen pair correlation function for both $1/r^9$ repulsive (Fig. 5a, Fig. 5b) and WCA (Fig. 5c, Fig. 5d) confinements. For both repulsive confinements, the qualitative behavior of the dependence of $g_{\parallel}$ is the same. At low temperature and low density, the first two peaks in $g_{\parallel}$ appear at $r = 2.78$ Åand $r = 4.5$ Å, but at high densities the second peak moves to a larger distance. This behavior is nearly identical to that observed for water confined between LJ surfaces, and is discussed in detail in Ref. [16].

We also confirm the structural similarity with LJ confinement by calculating the lateral static structure factor $S_{\parallel}(q)$, defined as the Fourier transform of the lateral RDF $g_{\parallel}(r)$,

$$S_{\parallel}(q) \equiv \frac{1}{N} \sum_{j,k} \left\langle e^{i\vec{q} \cdot (\vec{r_j} - \vec{r_k})} \right\rangle. \qquad (3)$$

Here the q-vector is the corresponding wave vector in the xy plane and r is the projection of the position vector on the xy plane. In Fig. 6, we show the temperature and pressure dependence of lateral structure factors for both repulsive confinements. For both forms of repulsive confinement, the temperature and density dependence of $S_{\parallel}$ is similar. We find

that confined water has a weaker pre-peak at $\approx 18\text{nm}^{-1}$ compared to bulk water (Fig. 7), consistent with the possibility that the local tetrahedrality is weakened by repulsive confinements. Of the three forms of confinement, the $S_\parallel$ for LJ confinement is most like bulk water (Fig. 7). Local tetrahedrality becomes weaker in case of repulisive confinements compared to LJ confinement. Further, we see that the water in $1/r^9$ repulsive confinement is less structured in lateral directions compared to water in WCA confinement, indicated by a less sharp and broad pre-peak at $\approx 18 \text{ nm}^{-1}$ in $S_\parallel(q)$ (Fig. 7).

IV. FREEZING OF TIP5P WATER

Bulk TIP5P water crystallizes within the simulation time for $\rho \gtrsim 1.15 \text{ g/cm}^3$ at low temperatures [36]. Crystallization of confined water is seen in some simulations [2, 6, 16]. A similar crystallization appears in simulations when an electric field is applied in lateral directions to a system of water confined between silica walls [15].

At plate separation of 1.1 nm with hydrophobic LJ confinement, water crystallizes to trilayer ice [16]. From our simulations of TIP5P water in repulsive confinements with the same plate separation of 1.1 nm, we find that the system does not freeze within accessible simulation time scales for $1/r^9$ repulsive confinement; however the system freezes for WCA confinement. As a more stringent confirmation of this fact, we also use a starting ice configuration obtained from simulations with LJ confinement for the same thickness, and confirm that the ice melts to a liquid with $1/r^9$ repulsive confinement. In Fig. 8, we show the evolution of potential energy and lateral structure factor with time, when the crystal formed in LJ confinement [16] is kept between the $1/r^9$ repulsive walls. The potential energy first increases and then reaches its equilibrium value of the liquid potential energy accompanied by a structural change from a crystal (presence of sharp Bragg peaks) to a liquid (absence of Bragg peaks).

Based on this observation, it is tempting to claim that repulsion inhibits crystallization, and that a preferable distance from the wall determined by the attractive portion of the LJ potential is necessary to induce crystallization. However, as discussed above for the same plate separation 1.1 nm, $1/r^9$ repulsive confinement with the chosen parameters increases the available space for molecules relative to LJ confinement. Hence to properly compare the crystallization behavior, we must adjust the separation of the wall so that the available

space for the water molecules is the same in both systems. We can make the available space the same by tuning the separation of the plates or by tuning the potential. By tuning the parameters (see Fig. 2, where the values of parameter ϵ_{OW} and σ_{OW} for the modified $1/r^9$-repulsive potential are 1.25 kJ/mol and 0.23 nm respectively) of the $1/r^9$ repulsive potential in the repulsive system such that the density profile along the z-axis becomes similar, we have identical values of the available space between the plates (see Fig. 9), and we find that an initial crystal configuration does *not* melt, emphasizing that the presence of the crystal is very sensitive to density *and* to plate separation – since the separation determines the accessible packing arrangements between the plates. Similar sensitivity to plate separation for monolayer ice was seen in ref. [15].

In addition to examining the stability of initially crystalline structures, we also consider whether freezing from the liquid state occurs when we have the same effective plate separation. We find that for the repulsively confined systems, the crystal will also spontaneously form if the available space between the plates is the same as that for which initially crystalline configurations are stable. Hence plate separation appears to be the dominant cause in determining whether or not a crystal will form.

V.   ACKNOWLEDGMENTS

[1] M.-C. Bellisent Funnel, ed., *Hydration Processes in Biology: Theoretical and Experimental Approaches* [NATO ASI Series A, Vol. 305] (IOS Press, Amsterdam, 1998).

[2] K. Koga, X. C. Zeng, and H. Tanaka, Phys. Rev. Lett. **79**, 5262 (1997).

[3] K. Koga, H. Tanaka, and X. C. Zeng, Nature **408**, 564 (2000).

[4] K. Koga and H. Tanaka, J. Chem. Phys. **122**, 104711 (2005).

[5] R. Zangi, J. Phys. Cond. Mat. **16**, S5371 (2004).

[6] R. Zangi and A. E. Mark, Phys. Rev. Lett. **91**, 0255502 (2003).

[7] J.-M. Zanotti, M.-C. Bellissent-Funel, and S.-H. Chen, Phys. Rev. E **59**, 3084 (1999).

[8] L. Liu, S.-H. Chen, A. Faraone, C.-W Yen, and C.-Y Mou, Phys. Rev. Lett. **95**, 117802 (2005).

[9] M.-C. Bellissent-Funel, R. Sridi-Dorbez, and L. Bosio, J. Chem. Phys. **104**, 10023 (1996).

[10] L. Xu, P. Kumar, S. V. Buldyrev, S.-H. Chen, P. Poole, F. Sciortino, and H. E. Stanley, Proc. Nat. Acad. Sci. **102**, 16558(2005).

[11] P. Kumar, L. Xu, Z. Yan, M. Mazza, S. V. Buldyrev, S.-H. Chen, S. Sastry, and H. E. Stanley (submitted).

[12] M. Antognozzi, A. D. L. Humphris, and M. J. Miles, Applied Physics Letters **78**, 300 (2001).

[13] J. J. Gilijamse, A. J. Lock, and H. J. Bakker, Proc. Nat. Acad. Sci. **102**, 3202 (2005).

[14] S Singh, J. Houston, F. V. Swol, and C. J. Brinker, Nature **442**, 526 (2005).

[15] R. Zangi and A. E. Mark, J. Chem. Phys. **119**, 1694 (2003); *ibid*, **120**, 7123 (2004).

[16] P. Kumar, S. V. Buldyrev, F. W. Starr, N. Giovambattista, and H. E. Stanley, Phys. Rev. E **72**, 051503 (2005).

[17] N. Giovambattista, P. Rossky, P. G. Debenedetti, Phys. Rev. E. (in press), (2006).

[18] J. Marti, G. Nagy, M. C. Gordillo, E. Guärdia, J. Chem. Phys. **124**, 094703 (2006).

[19] P. Gallo, M. Rovere, and E. Sphor **85** 4317 (2000).

[20] P. G. Debenedetti, J. Phys. Cond. Mat. **15**, R1669 (2003).

[21] P. G. Debenedetti and H. E. Stanley, Physics Today **56** (6), 40 (2003).

[22] C. A. Angell, Ann. Rev. Phys. Chem. **55**, 559 (2004).

[23] M. Meyer and H. E. Stanley, J. Phys. Chem. B **103**, 9728 (1999).

[24] W. L. Jorgensen, J. Chandrasekhar, J. Madura, R. W. Impey and M. Klein, J. Chem. Phys. **79**, 926 (1983).

[25] T. M. Truskett, P. G. Debenedetti, and S. Torquato, J. Chem. Phys. **114**, 2401 (2001).

[26] C. Rhykerd, M. Schoen, D. Diester, and J. Cushman, Nature (London) **330**, 461 (1989); P. A. Thompson and M. O. Robbins, Science **250**, 792 (1990).

[27] B. Brushan, J. N. Israelachvili, and U. Landman, Nature (London) **374**, 607 (1995).

[28] B. N. J. Persson, *Sliding Friction: Physical Principles and Application*, (Springer, Heidelberg, 1998).

[29] A. M. Homola, J. N. Israelachvili, M. L. Gee, and P. M. McGuiggan, J. Tribology **111**, 675 (1989); J. N. Israelachvili, Surf. Sci. Rep. **14**, 109 (1992).

[30] P. Gallo, M. Rovere and E. Spohr, J. Chem. Phys. **113**, 11324 (2000).

[31] P. Gallo, Phys. Chem. Chem. Phys. **2**, 1607 (2000).

[32] J. D. Weeks, D. Chandler, and H. C. Anderson, J. Chem. Phys **54**, 5237 (1971).

[33] M. W. Mahoney and W. L. Jorgensen, J. Chem. Phys. **112**, 8190 (2000).

[34] F. H. Stillinger and A. Rahman, J. Chem. Phys. **60**, 1545 (1974).

[35] Two positive point charges of charge $q_H = 0.241e$ (where e is the fundamental unit of charge) are located on each hydrogen atom at a distance 0.09572 nm from the oxygen atom; together they form an HOH angle of 104.52°. Two negative point charges ($q_e = -q_H$) representing the lone pair of electrons (e^-) are located at a distance 0.07 nm from the oxygen atom. These negative point charges are located in a plane perpendicular to the HOH plane and form an e^-Oe^- angle of $\cos^{-1}(1/3) = 109.47°$, the tetrahedral angle. To prevent overlap of molecules, a fifth interaction site is located on the oxygen atom, and is represented by a LJ potential with parameters $\sigma_{OO} = 0.312$ nm and $\epsilon_{OO} = 0.6694$ kJ/mol.

[36] M. Yamada, S. Mossa, H. E. Stanley, and F. Sciortino, Phys. Rev. Lett. **88**, 195701 (2002).

[37] M. W. Mahoney and W. L. Jorgensen, J. Chem. Phys. **114**, 363 (2001).

[38] J. M. Sorenson, G. Hura, R. M. Glaeser, and T. Head-Gordon, J. Chem. Phys. **113**, 9149 (2000).

[39] P. Kumar, S. V. Buldyrev, and H. E. Stanley, in *Soft Matter under Extreme Pressures: Fundamentals and Emerging Technologies* Editors: Sylwester J. Rzoska, Victor Mazur [Proc. NATO ARW, Odessa, Oct 2005] (Springer, Berlin, 2006).

[40] L. A. Baez and P. Clancy, J. Chem. Phys. **103**, 9744 (1995).

[41] H. J. C. Berendsen, J. P. M. Postma, W. F. van Gunsteren, A. DiNola and J. R. Haak, J. Chem. Phys. **81**, 3684 (1984).
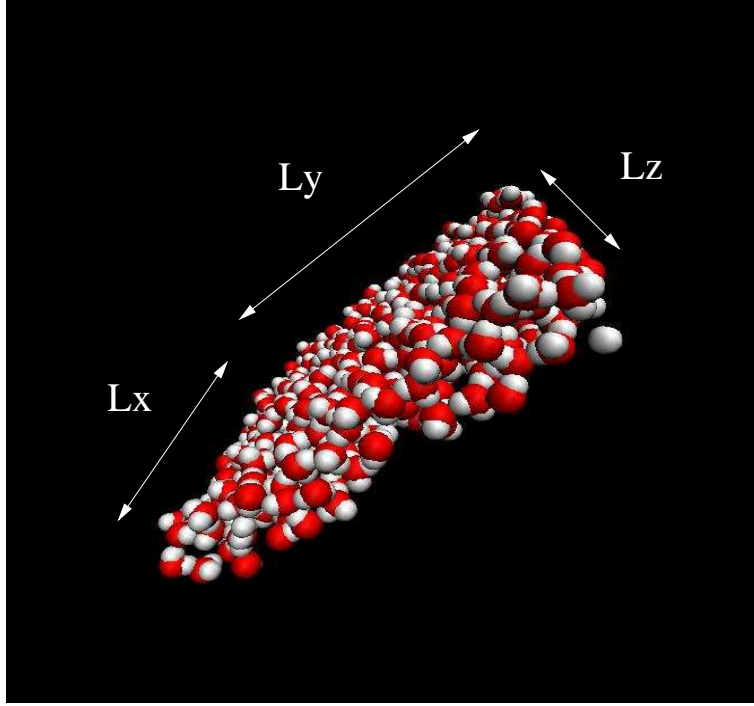
FIG. 1: Perspective view of the system, showing the 512 water molecules confined between two walls perpendicular to the z-direction. Note that the confining plates are located along the z-direction and are separated by 2-3 molecular layers of water.
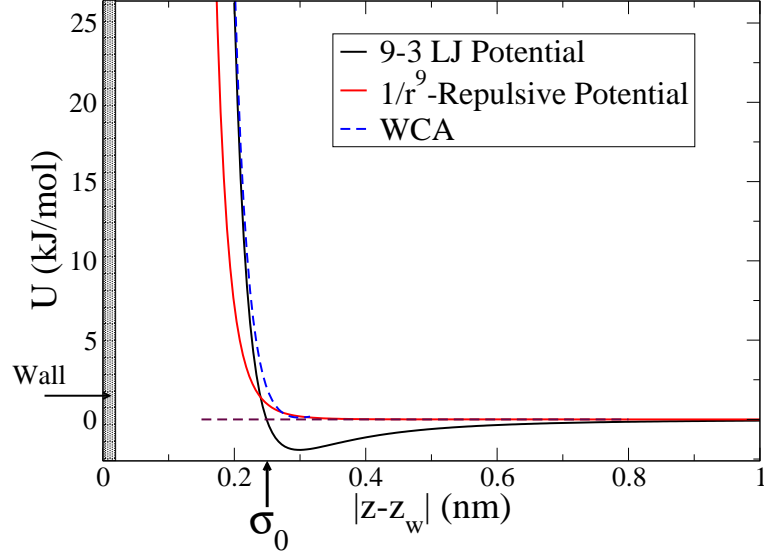
FIG. 2: Water-wall interaction potentials namely the 9-3 LJ, $1/r^9$ repulsive, and WCA potential as a function of distance of water molecules $|z - z_w|$ from the center of one of the walls (shaded rectangle).
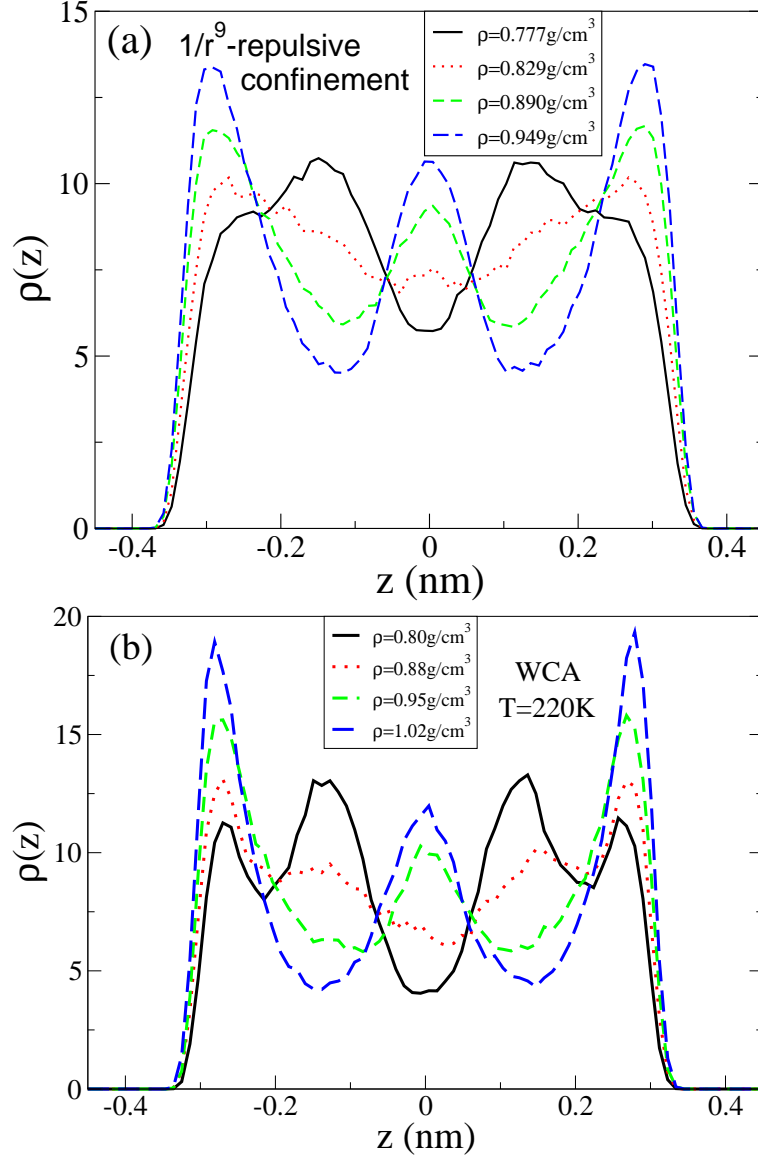
FIG. 3: Density profile $\rho(z)$ along z-direction for four different bulk densities at T=250 K for $1/r^9$ repulsive confinement. (b) Density profile $\rho(z)$ along z-direction for four different bulk densities at T=220 K for the case of WCA confinement. Both the repulsive confinements show similar layering of water molecules as seen in the case of LJ confinement [6, 16].
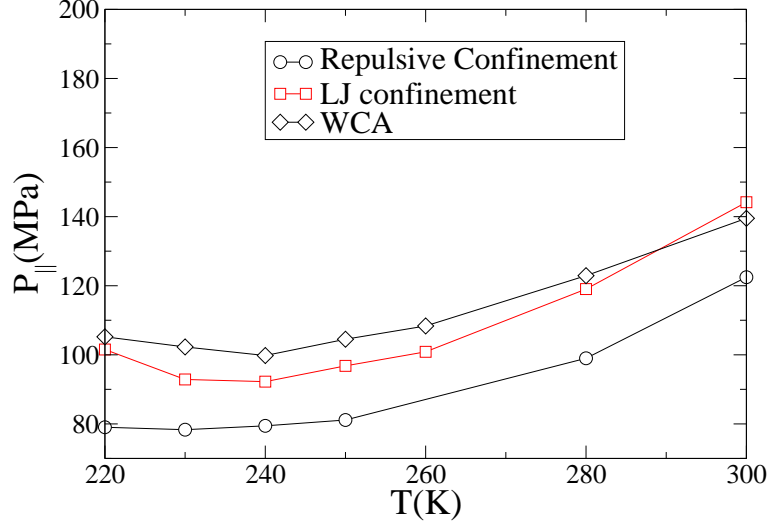
FIG. 4: Lateral pressure $P_{\parallel}$ for one isochore for the purely repulsive, LJ confinement and WCA cases. Here the effective density is $\rho = 0.829$ g/cm^3 for the $1/r^9$ repulsive potential and $\rho = 0.950$ g/cm^3 for LJ confinement. These effective densities for both systems correspond to the same geometric density of $\rho_{\mathrm{g}} = 0.709$ g/cm^3. All forms of confinement show a TMD, indicated by the minimum of the pressure; however the TMD is very "flat" for $1/r^9$ repulsive and WCA confinement. As expected the value of $P_{\parallel}$ approaches the value of $P_{\parallel}$ for the case of LJ confinement at high temperatures.
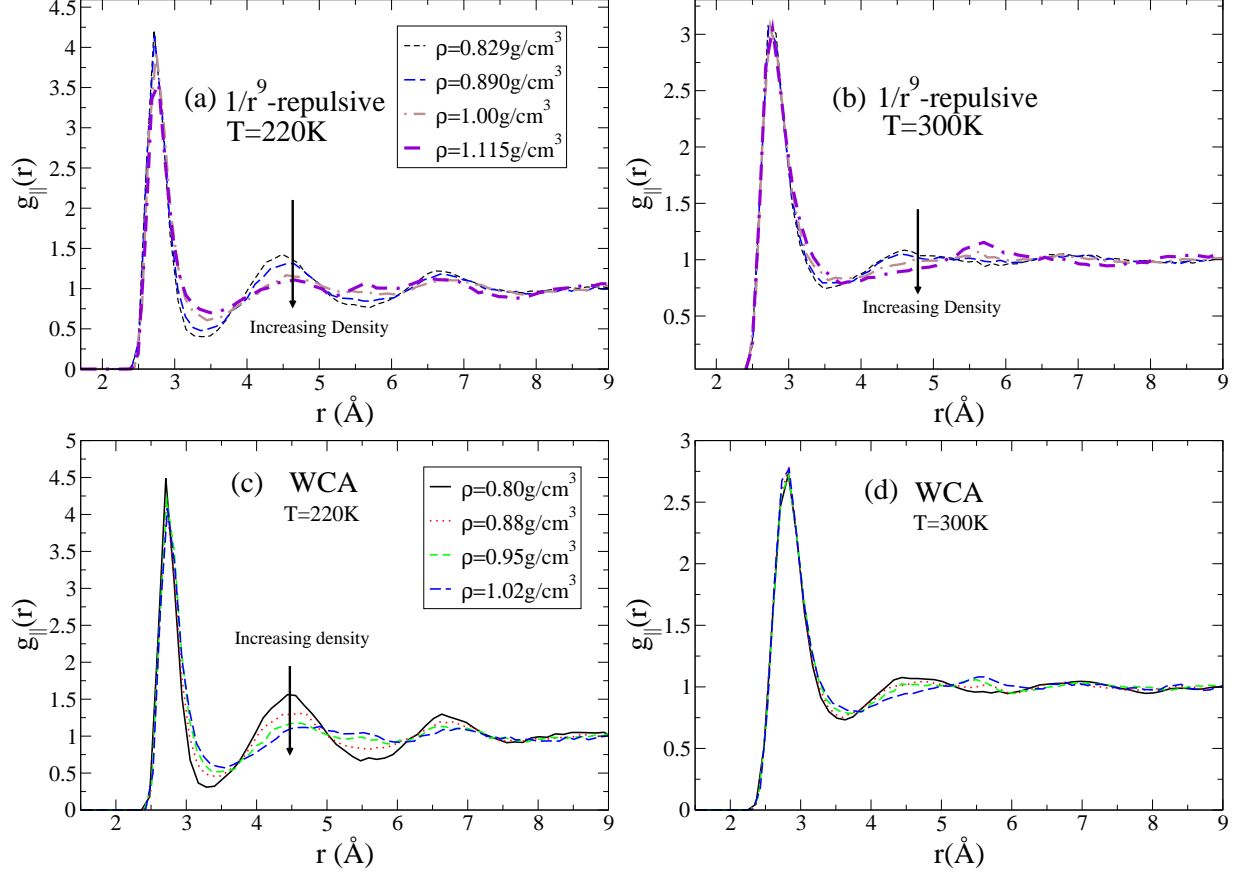
FIG. 5: Lateral oxygen-oxygen pair correlation function $g_\parallel(r)$ for the case of $1/r^9$ repusive and WCA confinements. Shown are four different densities at two fixed temperatures (a) $T = 220$ K and (b) $T = 300$ K for $1/r^9$ repulsive confinement and (c) and (d) for WCA confinement. Note that with increasing density, the second neighbor peak at ≈ 0.45 nm becomes less pronounced and at high temperatures moves to a larger distance seen in LJ confinement [16].
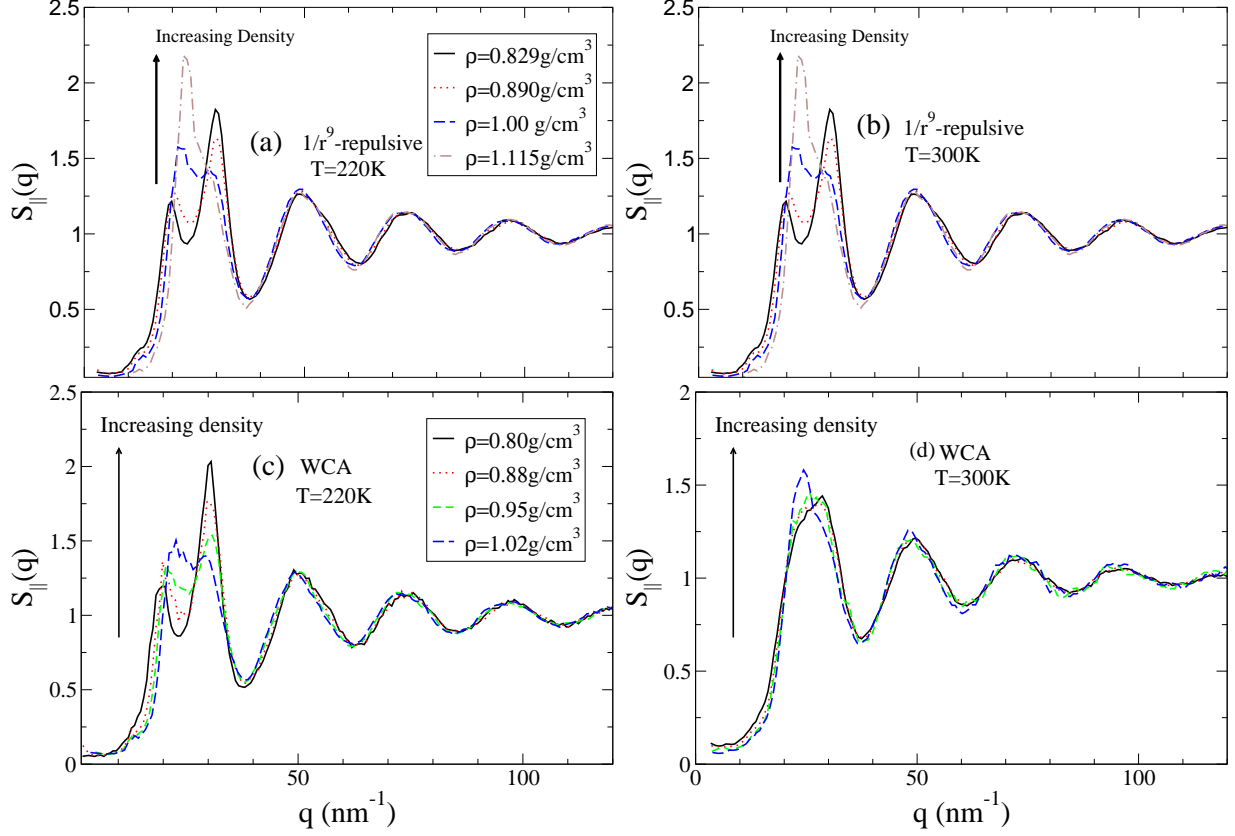
FIG. 6: Lateral structure factor $S_{\parallel}(q)$ for the case of $1/r^9$ repulsive and WCA confinements. Shown are four different densities at two fixed temperatures (a) $T = 220$ K and (b) $T = 300$ K for $1/r^9$ repulsive confinement and (c) and (d) for WCA confinement for the same temperatures. The first peak of $S_{\parallel}(q)$ corresponding to the hydrogen-bonds weakens as density is increased and is absent at high densities and high temperatures. The first peak of $S_{|}(q)$ in the case of $1/r^9$ repulsive confinement weaker than the LJ confinement.
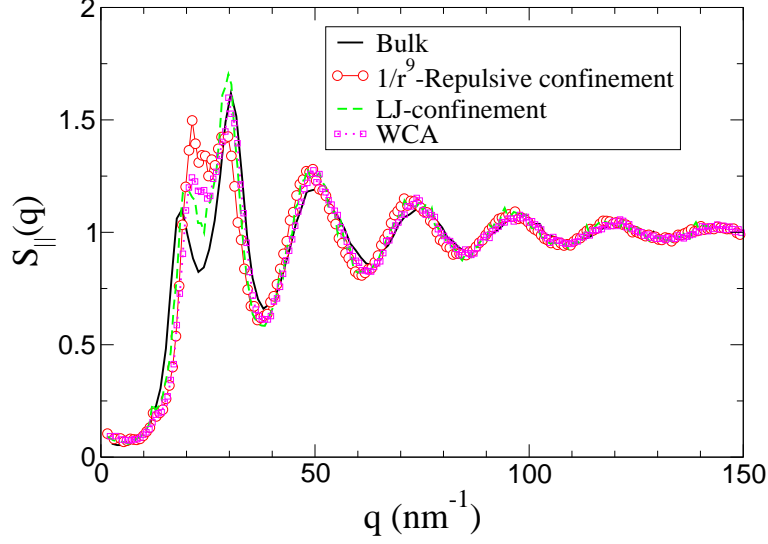
FIG. 7: A comparison of the structure factors for different confinements with bulk water structure factor at T=250K. For the comparion we choose the effective densities in confinements close to each other. Densities for $1/r^9$ repulsive confinement, LJ confinement, WCA-confinement are chosen to be 0.950 g/cm^3. We choose the structure factor for bulk water at density 1.00 g/cm^3 . A diminished peak at ≈ 18 nm^{-1} shows that the local tetrahedral structure is weakened in case of all forms of confinement. A further comparison of LJ confinement at 0.950 g/cm^3 with $1/r^9$ repulsive confinement shows that water in $1/r^9$ repulsive confinement is less tetrahedral, as the first peak of $S_\parallel(q)$ is much weaker than the first peak of $S_\parallel(q)$ for LJ confinement. Water in WCA confinement is more structured than $1/r^9$ repulsive confinement, but is less structured than LJ confinement.
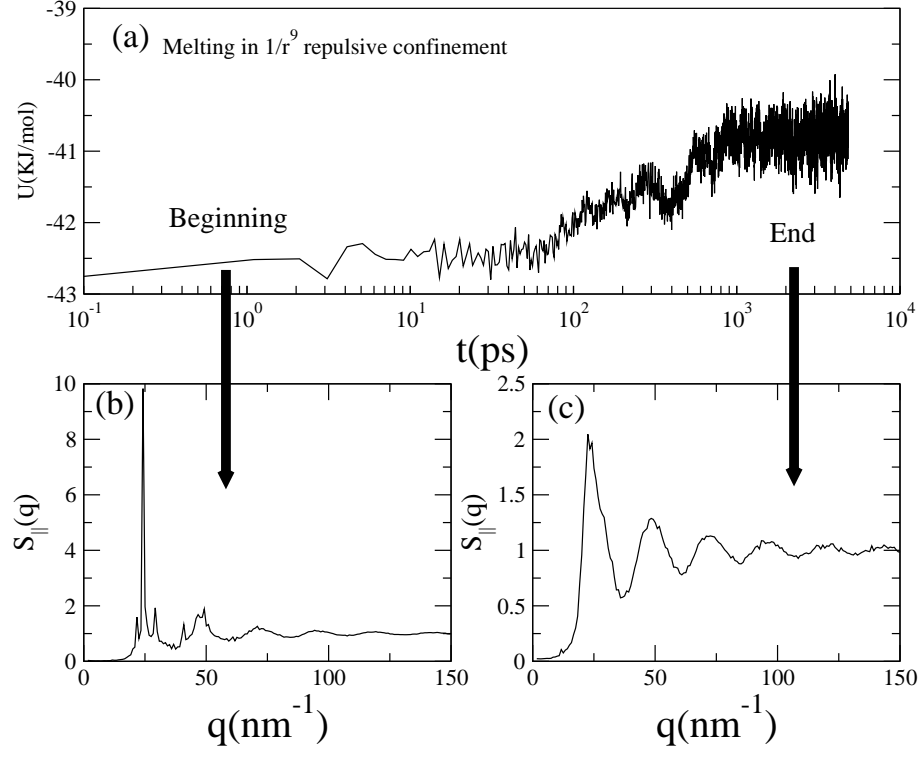
FIG. 8: (a) A plot of potential energy as a function of t, when the crystal formed in LJ confinement [16] is kept between the $1/r^9$ repulsive wall. (b) The crystal structure indicated by the sharp Bragg peaks melts, and (c) turns into a liquid indicated by the absence of Bragg peaks.
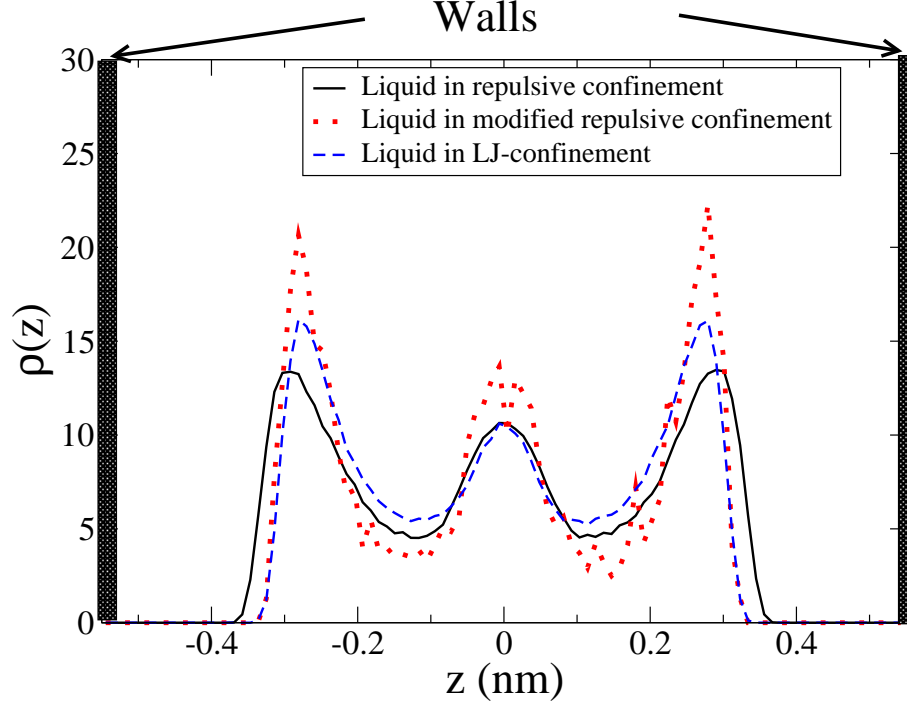
FIG. 9: Density profile $\rho(z)$ of water along z-direction for different potentials at the same geometric density. The repulsive confinement system freezes spontaneously when the parameters of the potential are modified such that the effective L_z calculated from the $\rho(z)$ (red dotted line) for the repulsive system is same as that for the LJ system (blue-dashed line) (see Fig. 2).
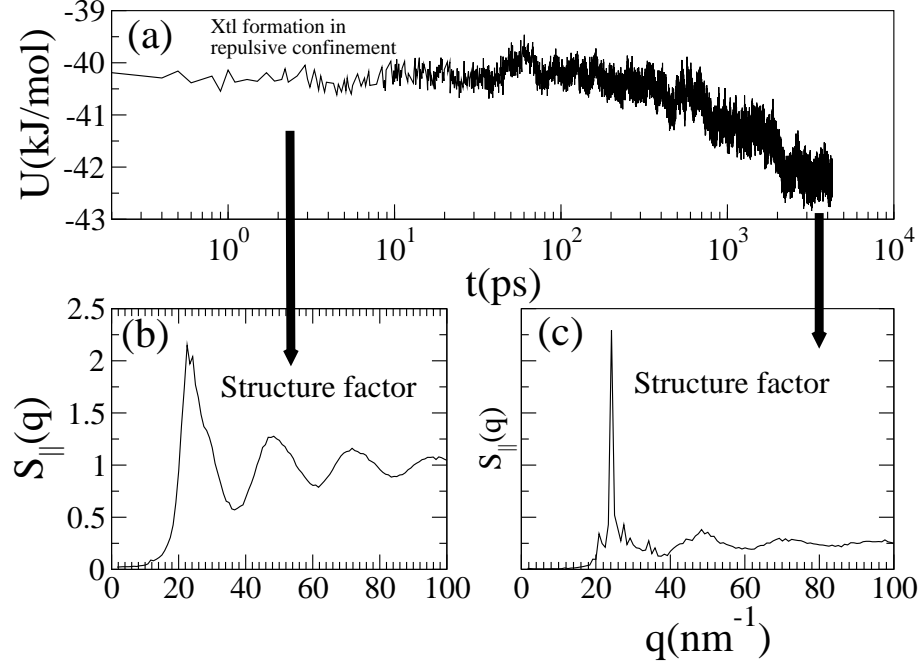
FIG. 10: (a) Potential energy as a function of time t, for $1/r^9$ repulsive confinement when the effective L_z is same as the effective L_z of LJ confinement at $T = 260$ K and geometric density $\rho_g = 0.981$ g/cm^3. The confined water spontaneously freezes, indicated by the drop in potential energy. (b) The structure factor of the ice such formed resembles the trilayer ice seen in case of LJ confinement [6, 16].